metals

MDPI

Article

Tensile Fracture Behavior of Progressively-Drawn Pearlitic Steels

Jesús Toribio *, Francisco-Javier Ayaso, Beatriz González, Juan-Carlos Matos, Diego Vergara and Miguel Lorenzo

Fracture & Structural Integrity Research Group, University of Salamanca, E.P.S., Campus Viriato, Avda. Requejo 33, Zamora 49022, Spain; fja@usal.es (F.-J.A.); bgonzalez@usal.es (B.G.); jcmatos@usal.es (J.-C.M.); dvergara@usal.es (D.V.); mlorenzo@usal.es (M.L.)

* Correspondence: toribio@usal.es; Tel.: +34-980-545-000 (ext. 3673); Fax: +34-980-545-002

Academic Editor: Isabel Gutierrez

Received: 31 March 2016; Accepted: 10 May 2016; Published: 17 May 2016

Abstract: In this paper a study is presented of the tensile fracture behavior of progressively-drawn pearlitic steels obtained from five different cold-drawing chains, including each drawing step from the initial hot-rolled bar (not cold-drawn at all) to the final commercial product (pre-stressing steel wire). To this end, samples of the different wires were tested up to fracture by means of standard tension tests, and later, all of the fracture surfaces were analyzed by scanning electron microscopy (SEM). Micro-fracture maps (MFMs) were assembled to characterize the different fractographic modes and to study their evolution with the level of cumulative plastic strain during cold drawing.

Keywords: cold drawing; pearlitic steel; steel wires; mechanical properties; tensile fracture; fractographic analysis; anisotropic behavior

1. Introduction

Pearlitic steels are widely used in a high variety of applications in engineering, e.g., pre-stressing steel wires [1,2], railway rails [3–5], rock bolts [6], steel cord wires (tire reinforcement) [7], music wires [8], *etc*. The wide use of these types of steels is due to their excellent mechanical properties induced in the raw material during the mechanical conforming process, e.g., hot rolling for complex shapes or wire drawing in the case of cylindrical bars. As a result of the plastic strains undergone by the material during the latter process, the yield stress is high enough [9] for considering it as a high strength steel. The today importance of these steels in industry can be quantified in terms of the world production of drawn wires of pearlitic steels which can be estimated in 25 million tons per year [10]. In addition, the interest of the scientific community on these research areas is also very high, as indicated by the number of research papers published up to date in multiple journals indexed in the SCOPUS database (Figure 1).

Consequently, from a pure scientific point of view, increasing the knowledge about pearlitic steel wires is a quite interesting issue. In a common commercial wire drawing chain, wires undergo a progressive reduction of their cross-sectional area during several steps (usually 6–8 passes) [11]. As a consequence of material hardening due to huge plastic strains in the wire, key microstructural changes are caused in the steels as was reported in many studies [12–19]. The analyses of such changes revealed a progressive increment of the microstructural anisotropy as the drawing degree is increased. These microstructural changes also affect the macroscopic mechanical behavior of the material [20–22], as in their fatigue and fracture behavior [23–27].

This paper goes further in the research, so that a study is presented of the tensile fracture behavior of progressively-drawn pearlitic steels obtained from five different real cold drawing chains, including each drawing step from the initial hot-rolled bar (not cold-drawn at all) to the final commercial product (pre-stressing steel wire).

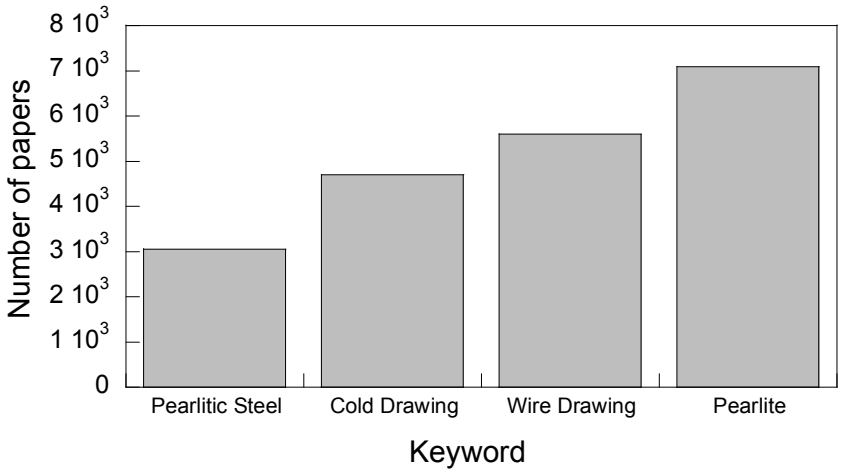

Figure 1. Number of research papers indexed in Scopus related with the following keywords: pearlitic steel, cold drawing, wire drawing, pearlite. (Data collected on February 2016).

For this purpose, standard tension tests up to final fracture were carried out for each one of the wires corresponding to each step of the five commercial wire drawing chains considered in this study. On one hand, results of testing allow one to obtain the mechanical properties—material yield strength (σ_Y) and ultimate tensile strength (UTS, σ_R)—of each one of the wires tested from the material constitutive law (stress-strain curve). This mechanical characterization presents a high interest not only from the scientific point of view, but also from the educational viewpoint [28]. On the other hand, the quantitative fractographic analysis (post mortem) of the fracture surfaces of tested samples, obtained by scanning electron microscopy (SEM), allows one to reveal the microscopic fracture maps (MFMs) and the fracture micro-mechanisms. From these analyses, the evolution of both mechanical properties and fracture behavior with drawing will be revealed for different wire drawing processes, thereby achieving a better understanding of the mechanical behavior of these key types of steels.

2. Experimental Program

Cylindrical samples of the wires obtained at the end of each drawing step of the five commercial manufacturing processes were used for testing. Each one of the families of progressively-drawn steels was labelled with a capital letter (A, B, C, D and E). In addition, to identify each particular steel (member of the family), a number was added representing the number of drawing steps undergone by the specific wire. Thus, as a way of example, steel E4 corresponds to a wire obtained after the fourth drawing step of family E. According to Table 1, the chemical composition of the five families of steels is similar with slight variations.

Table 1. Chemical composition of the five families of steels.

Element	Family of Steels				
	A	**B**	**C**	**D**	**E**
% C	0.800	0.789	0.790	0.795	0.789
% Mn	0.690	0.698	0.670	0.624	0.681
% Si	0.230	0.226	0.200	0.224	0.210
% P	0.012	0.011	0.009	0.011	0.010
% S	0.009	0.005	0.009	0.008	0.008
% Al	0.004	0.003	0.003	0.003	0.003
% Cr	0.265	0.071	0.187	0.164	0.218
% V	0.060	0.078	0.053	0.064	0.061

Each one of the raw materials for each family undergoes different straining paths during the manufacturing process by cold drawing. Family A is forced to pass through six drawing dies, whereas the wire drawing of the other families (B, C, D and E) is divided into seven drawing steps. Table 2 summarizes each one of the five cold drawing procedures (straining paths or yielding histories) in terms of the wire diameter at the end of each drawing step.

Table 2. Diameter of the wires at the end of each drawing step for the five families.

Drawing Step	Wire Diameter (mm)				
	Family A	**Family B**	**Family C**	**Family D**	**Family E**
0	12.11	12.10	10.44	8.56	11.03
1	10.80	11.23	9.52	7.78	9.90
2	9.81	10.45	8.49	6.82	8.95
3	8.94	9.68	7.68	6.17	8.21
4	8.22	9.02	6.95	5.61	7.49
5	7.56	8.54	6.36	5.08	6.80
6	6.98	8.18	5.86	4.63	6.26
7	-	7.00	5.03	3.97	5.04

The cumulative plastic strain ε^P represents the drawing degree [23], and is defined as follows:

$$\varepsilon^P = 2\ln\frac{\phi_0}{\phi_i} \quad (1)$$

where ϕ_0 is the hot-rolled bar diameter (not cold drawn at all) and ϕ_i is the diameter of a wire undergoing i drawing steps. Results for the different drawn wires are given in Table 3.

Table 3. Cumulative plastic strain of the progressively drawn steels.

Drawing Step	ε^P				
	Family A	**Family B**	**Family C**	**Family D**	**Family E**
0	0	0	0	0	0
1	0.229	0.149	0.184	0.191	0.216
2	0.421	0.293	0.414	0.454	0.418
3	0.607	0.446	0.614	0.655	0.591
4	0.775	0.588	0.814	0.845	0.774
5	0.942	0.697	0.991	1.044	0.967
6	1.102	0.800	1.155	1.229	1.133
7	-	1.095	1.460	1.537	1.566

Standard tension tests were performed up to final fracture. Three tests were made for each drawing step (thus, as many as 117 standard tension tests were performed in the mechanical characterization, a huge collection of statistical quantitative data).

3. Microstructure of the Progressively-Drawn Wires

The microstructure of the progressively-drawn wires is given in Figures 2–5 (the vertical side of longitudinal sections always corresponds to the wire axis). They show a progressive slenderizing of the pearlitic colonies and an increase of packing closeness (with decrease of pearlite interlamellar spacing). In addition, a progressive orientation (in the drawing direction) of both pearlitic colonies (first microstructural level) and ferrite/cementite lamellae (second microstructural level) can be observed. All these observations are fully consistent with previous research in similar steels [12–15].

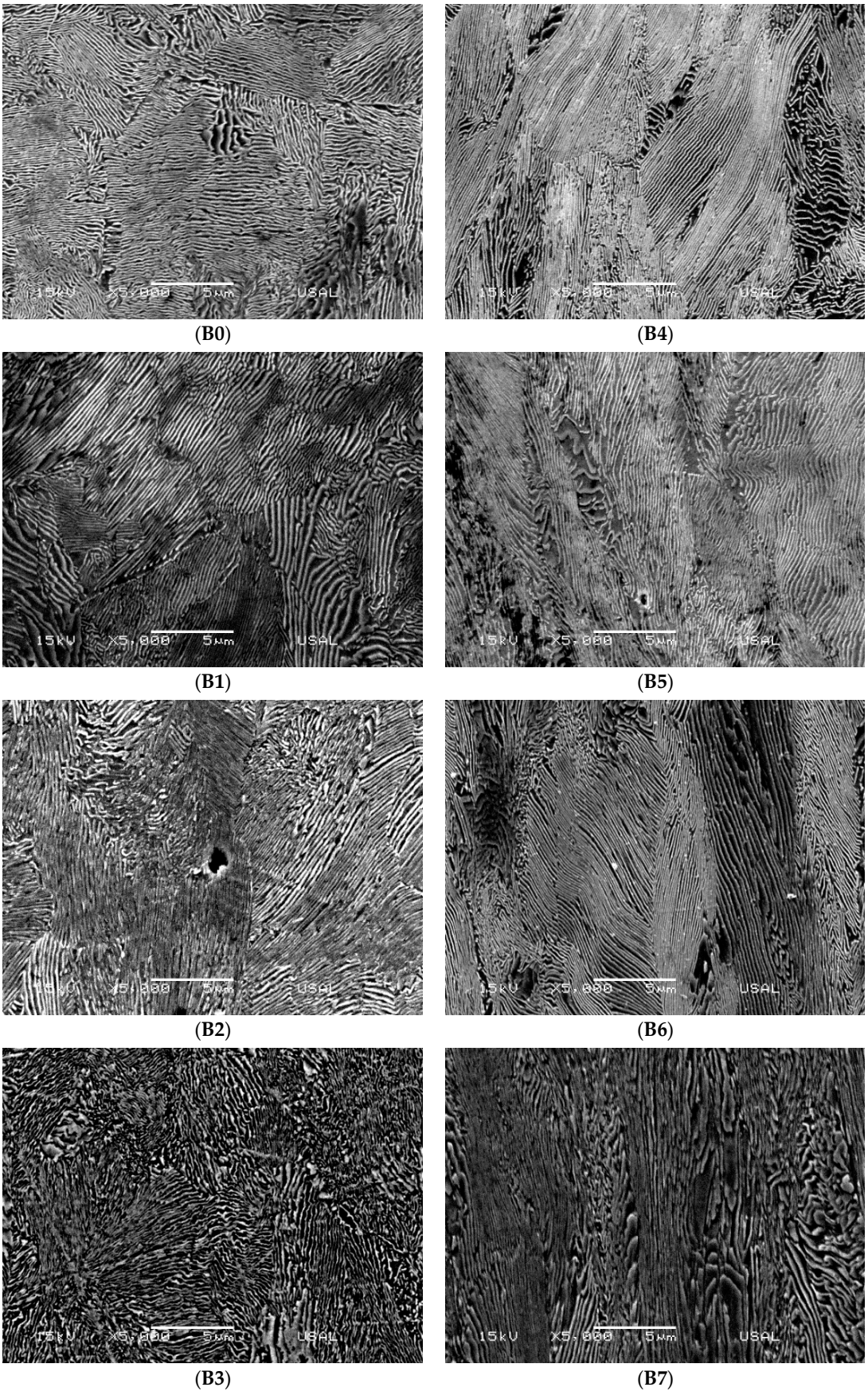

Figure 2. Metallographic analysis of the longitudinal section of family B for diverse drawing steps.

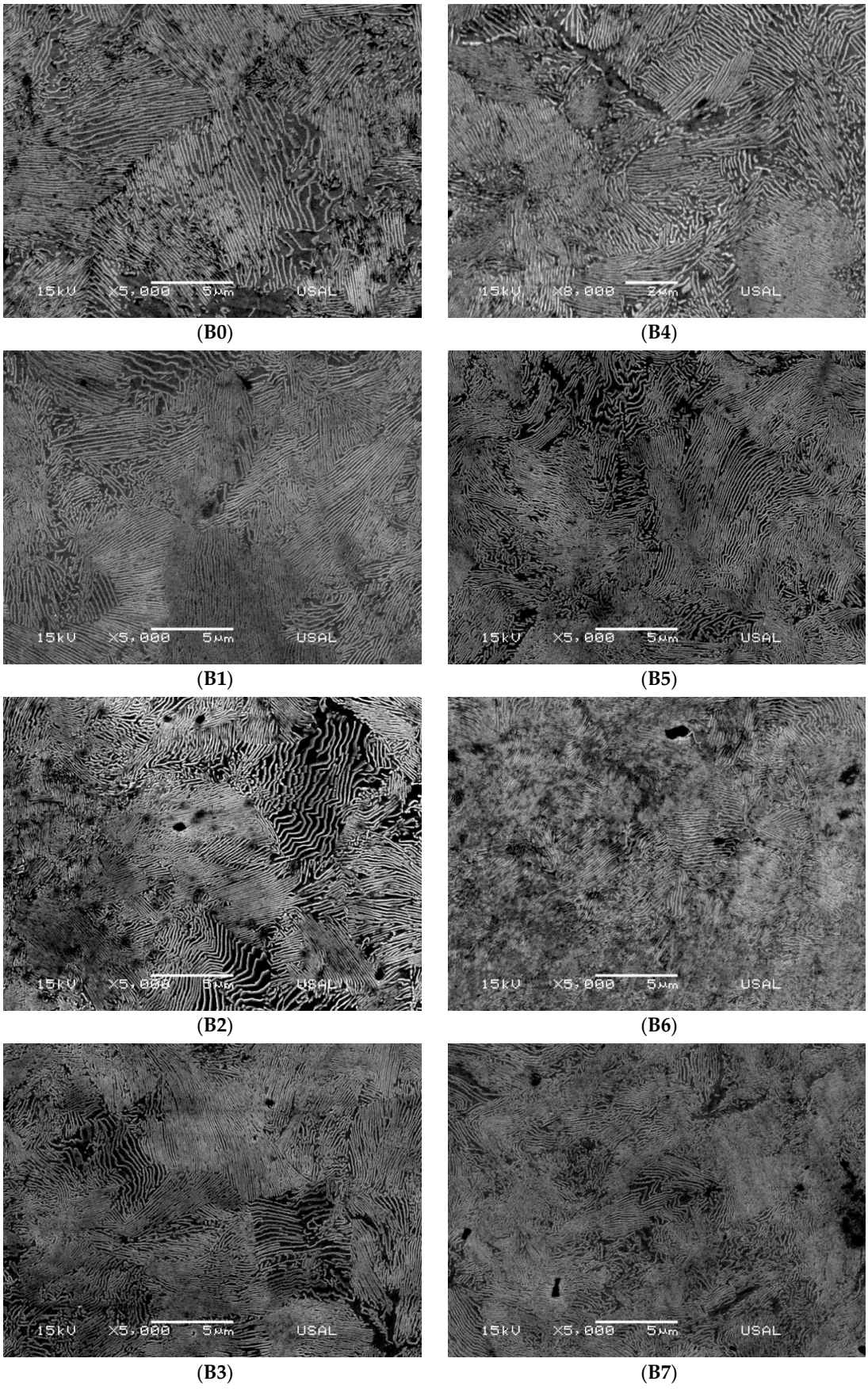

Figure 3. Metallographic analysis of the transverse section of family B for diverse drawing steps.

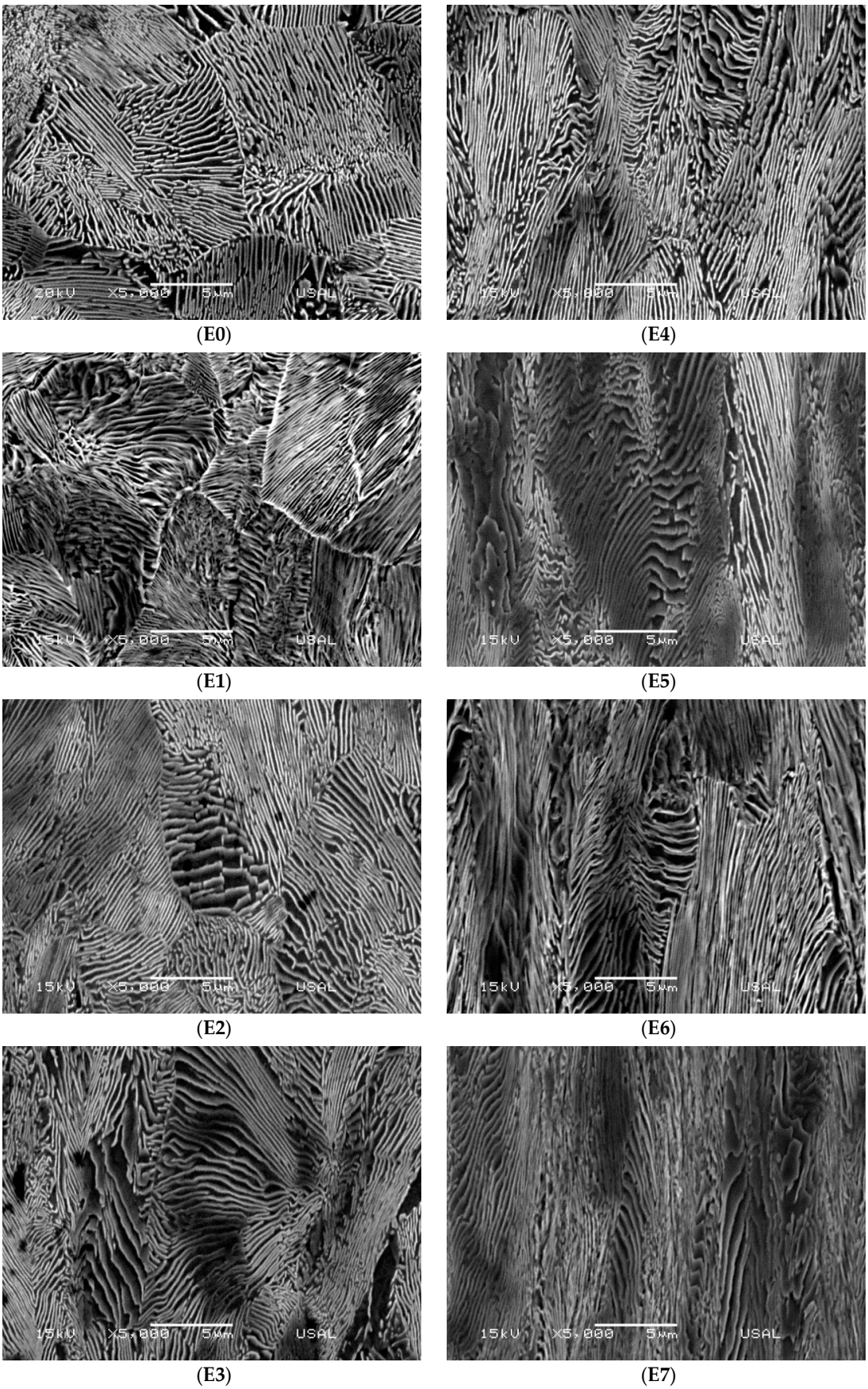

Figure 4. Metallographic analysis of the longitudinal section of family E for diverse drawing steps.

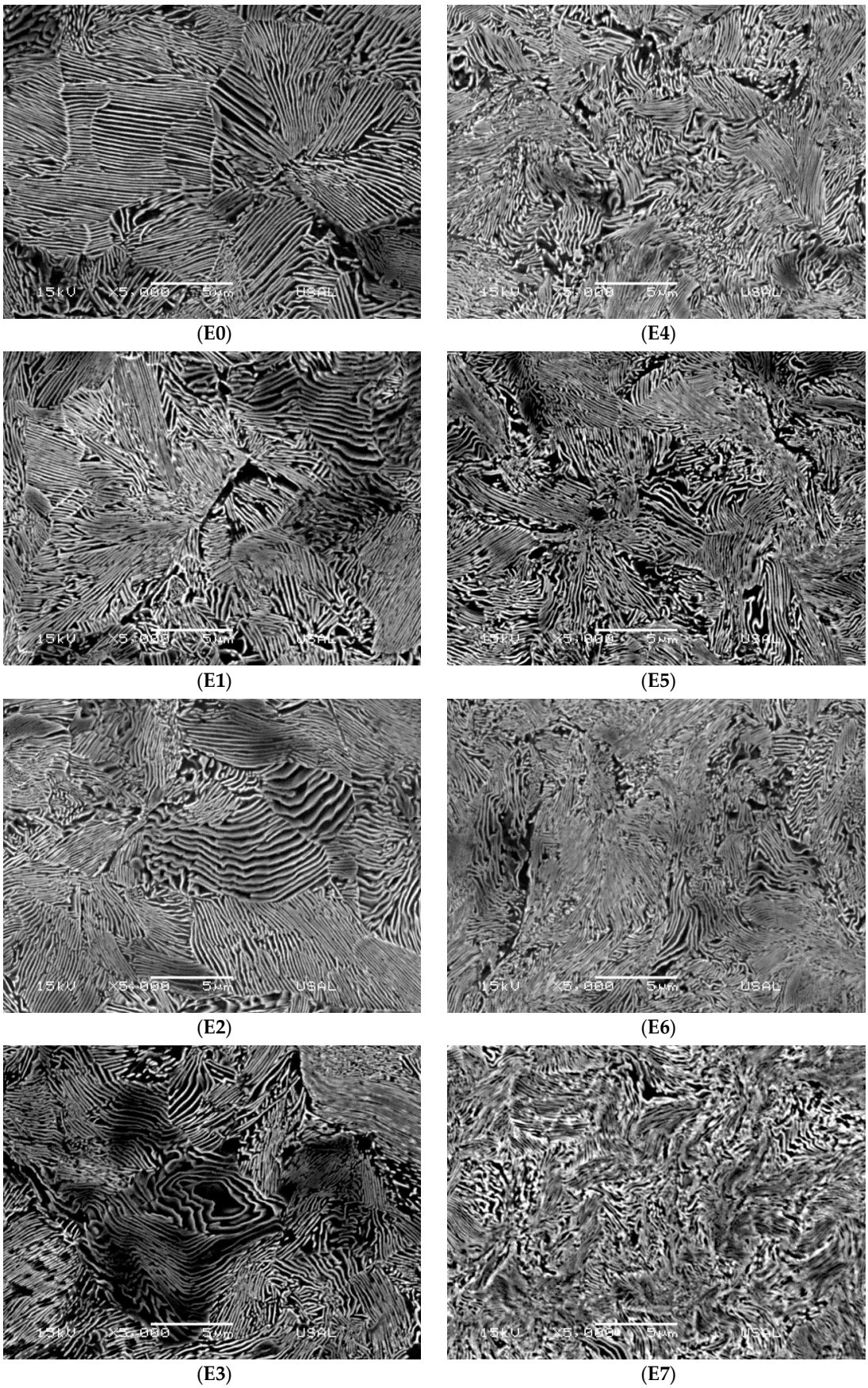

Figure 5. Metallographic analysis of the transverse section of family E for diverse drawing steps.

4. Mechanical Behavior of the Progressively-Drawn Wires

Conventional standard tension tests up to final fracture under a constant displacement rate of 2 mm/min were carried out using cylindrical samples of 300 mm length for each one of the drawing steps and the five families of steels used in the experimental program. Such a length was selected following the recommendation of a previous study [29]. Figure 6 shows the obtained master curves (stress *vs*. strain curves) as results of testing for each drawing step of the considered steels. Furthermore, Table 4 shows the values of the main mechanical properties of the previous steels.

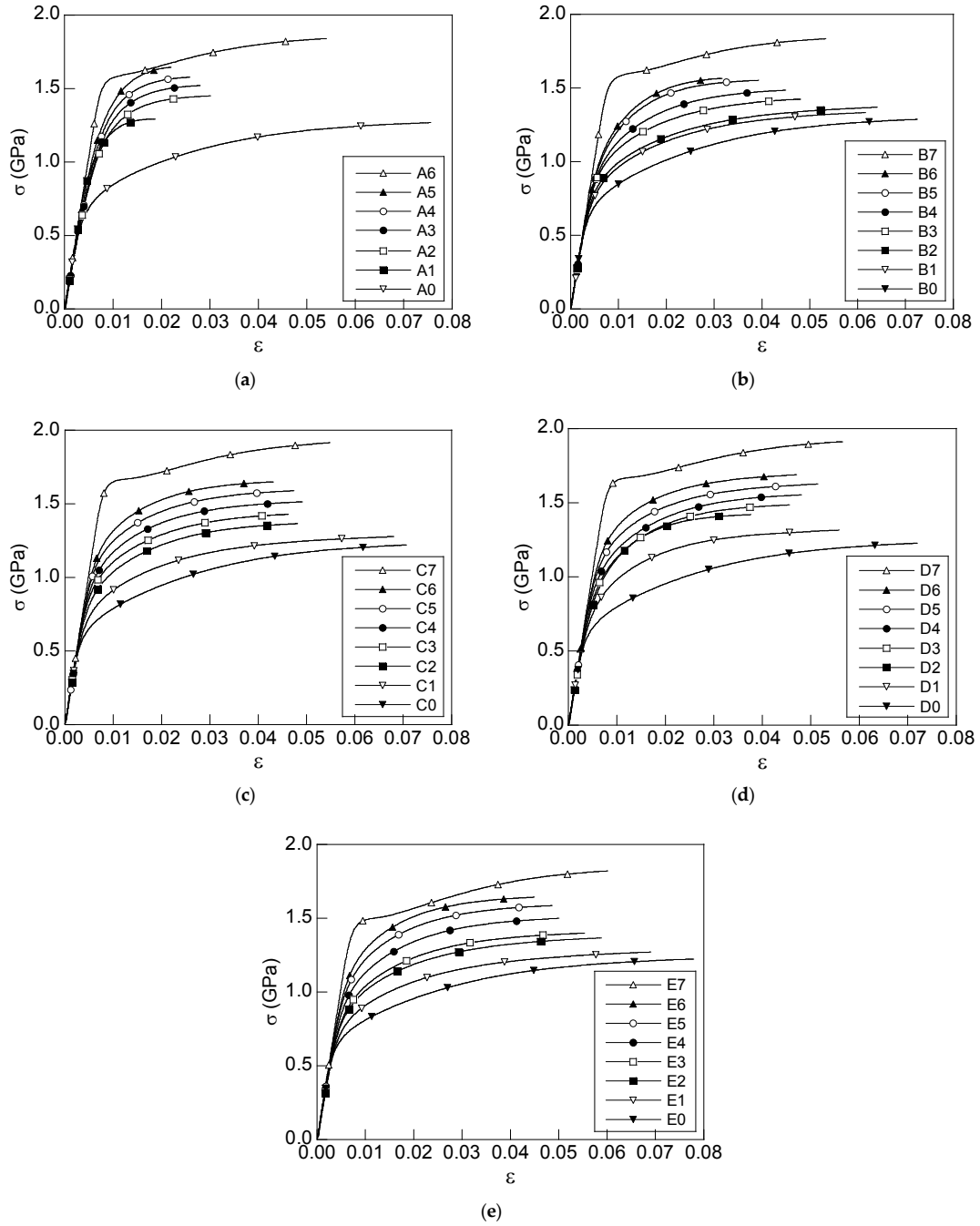

Figure 6. Stress-strain curves of the progressively-drawn steels: (**a**) family A with six drawing degrees; (**b**) family B with seven drawing degrees; (**c**) family C with seven drawing degrees; (**d**) family D with seven drawing degrees; and (**e**) family E with seven drawing degrees.

Table 4. Main mechanical properties for each drawing step of the considered families.

Steel	*E* (GPa)	σ_Y (GPa)	σ_R (GPa)	ε_R
Family A				
A0	194	0.72	1.27	0.076
A1	201	1.10	1.29	0.018
A2	187	1.12	1.45	0.030
A3	190	1.18	1.52	0.028
A4	190	1.26	1.58	0.026
A5	195	1.33	1.65	0.022
A6	207	1.57	1.84	0.054
Family B				
B0	202	0.72	1.27	0.066
B1	204	0.84	1.34	0.057
B2	204	0.88	1.37	0.061
B3	203	0.95	1.43	0.052
B4	203	1.01	1.49	0.042
B5	201	1.09	1.55	0.038
B6	201	1.12	1.58	0.035
B7	205	1.58	1.84	0.052
Family C				
C0	203	0.69	1.23	0.066
C1	199	0.78	1.27	0.061
C2	201	0.90	1.36	0.046
C3	204	0.97	1.42	0.047
C4	204	1.06	1.50	0.043
C5	204	1.14	1.58	0.045
C6	204	1.23	1.64	0.042
C7	208	1.65	1.91	0.051
Family D				
D0	194	0.68	1.23	0.072
D1	192	0.84	1.32	0.056
D2	189	0.99	1.42	0.038
D3	194	1.00	1.49	0.045
D4	200	1.07	1.55	0.048
D5	202	1.16	1.63	0.051
D6	202	1.25	1.69	0.047
D7	206	1.65	1.88	0.057
Family E				
E0	199	0.72	1.23	0.068
E1	192	0.83	1.28	0.056
E2	194	0.91	1.36	0.049
E3	192	0.93	1.41	0.055
E4	196	1.02	1.50	0.049
E5	199	1.13	1.60	0.048
E6	200	1.16	1.62	0.043
E7	208	1.49	1.83	0.059

E: Young modulus; σ_Y: yield strength; σ_R: ultimate tensile strength (UTS); ε_R: strain at maximum load.

From such curves (Figure 6), the mechanical properties can be determined and, thus, the evolution of yield strength σ_Y (Figure 7a) and ultimate tensile strength σ_R (Figure 7b) with the drawing degree is revealed in terms of cumulative plastic strain (ε^P).

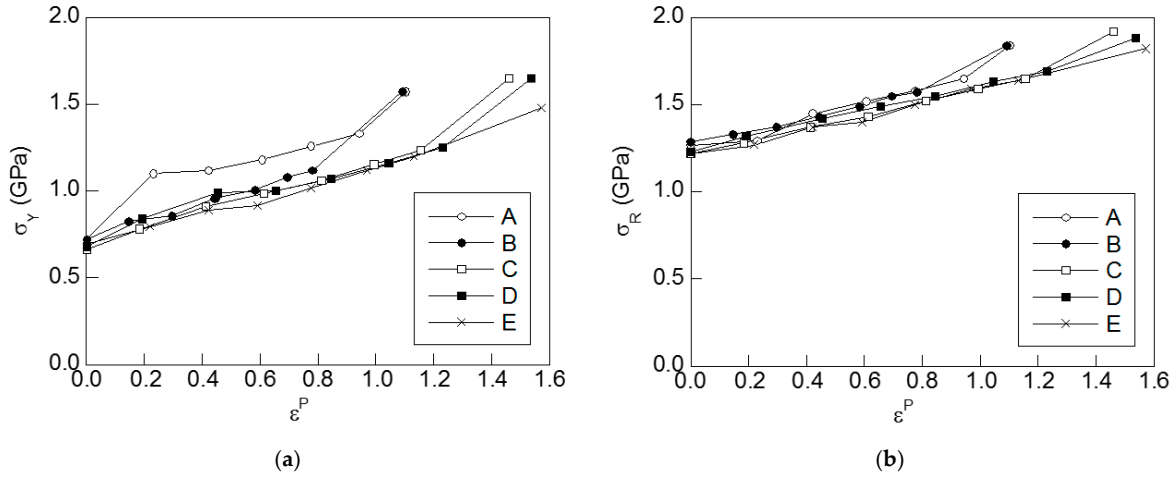

Figure 7. Mechanical properties evolution with cold drawing, for each one of the five pearlitic families of steels: (**a**) yield strength; (**b**) ultimate tensile strength (UTS).

As Figure 7a,b clearly show, a quasi-linear growing trend does exist in the yield strength and UTS with cumulative plastic strain during drawing. Therefore, a linear dependence seems to exist between both parameters and the drawing degree. In order to reveal such a dependence, a mathematical fitting (Figure 8) was applied to the data included in Figure 7a,b. The last step of wire drawing was not considered, since manufacturing companies used to apply a special heat treatment after the last drawing step for relieving the residual stresses induced by manufacturing. Thus, these equations mathematically represent the increment of yield strength and the UTS of pearlitic steels due to the strain hardening mechanism. These equations could be useful for obtaining a simple estimation of the material strength after a given straining process.

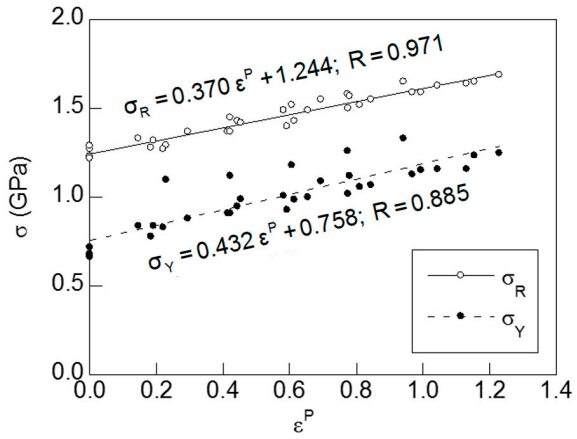

Figure 8. Mathematical fitting of the evolution of the mechanical properties (yield strength and UTS) with cumulative plastic strain of cold-drawn wires.

5. Fractographic Analysis

Fracture surfaces were observed by means of SEM. The fracture surface obtained after tensile testing of each drawing step of steel families B and E are shown in Figures 9 and 10 respectively. For each set of three tests (of the total amount of 117) a representative fracture surface was considered in the fractographic analysis. According to the MFMs, the slightly-drawn steels exhibit an isotropic fracture behavior and a smooth fracture surface at the macroscopic scale. As the drawing degree increases the mechanical behavior is modified (σ_Y and σ_R increase, Figure 8, and the fracture behavior,

too, showing a more irregular fractography with numerous peaks and valleys (strength anisotropy) as a consequence of the progressive microstructural orientation after manufacture.

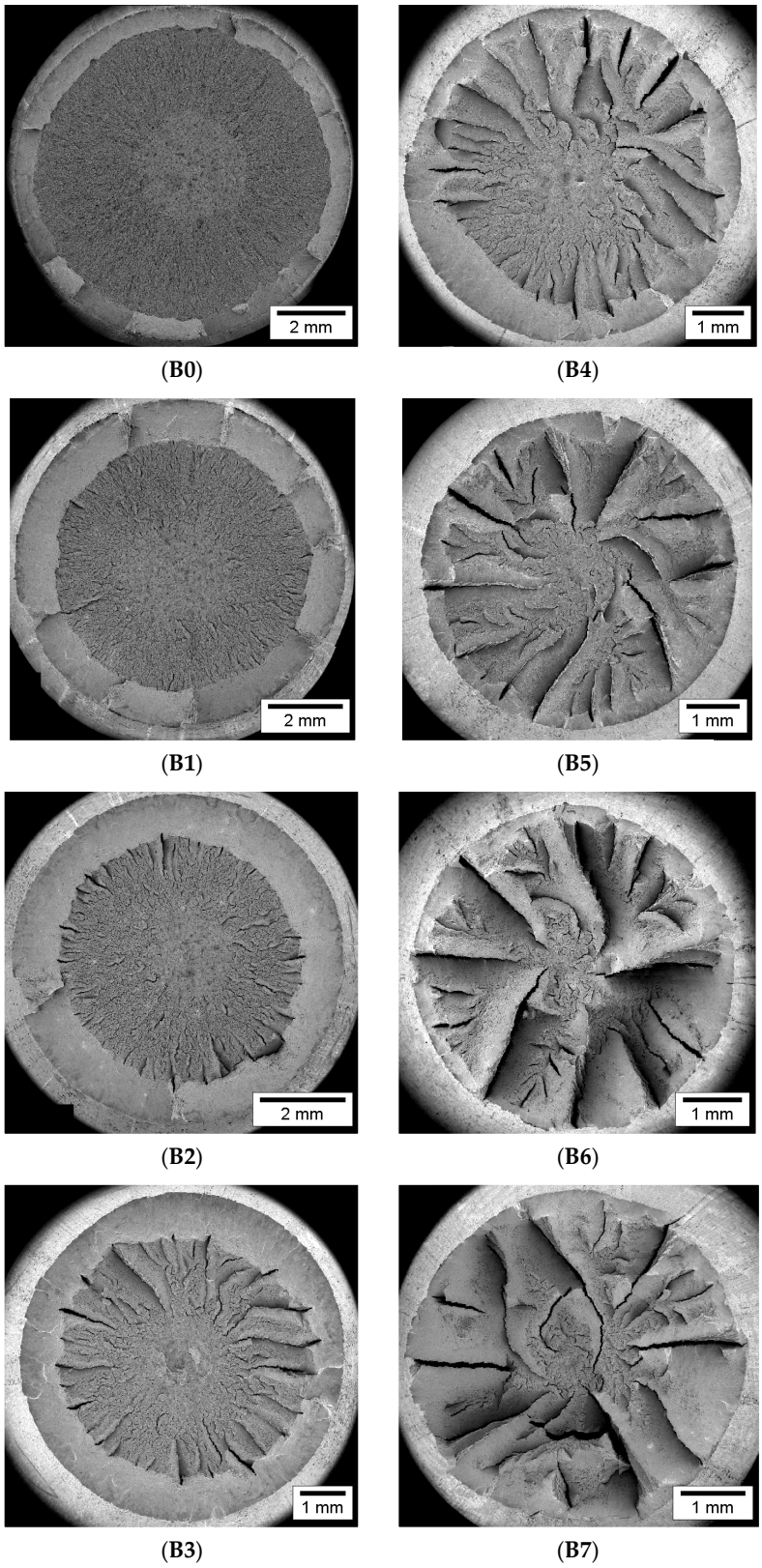

Figure 9. Evolution with drawing of MFMs of drawn wires corresponding to the family B.

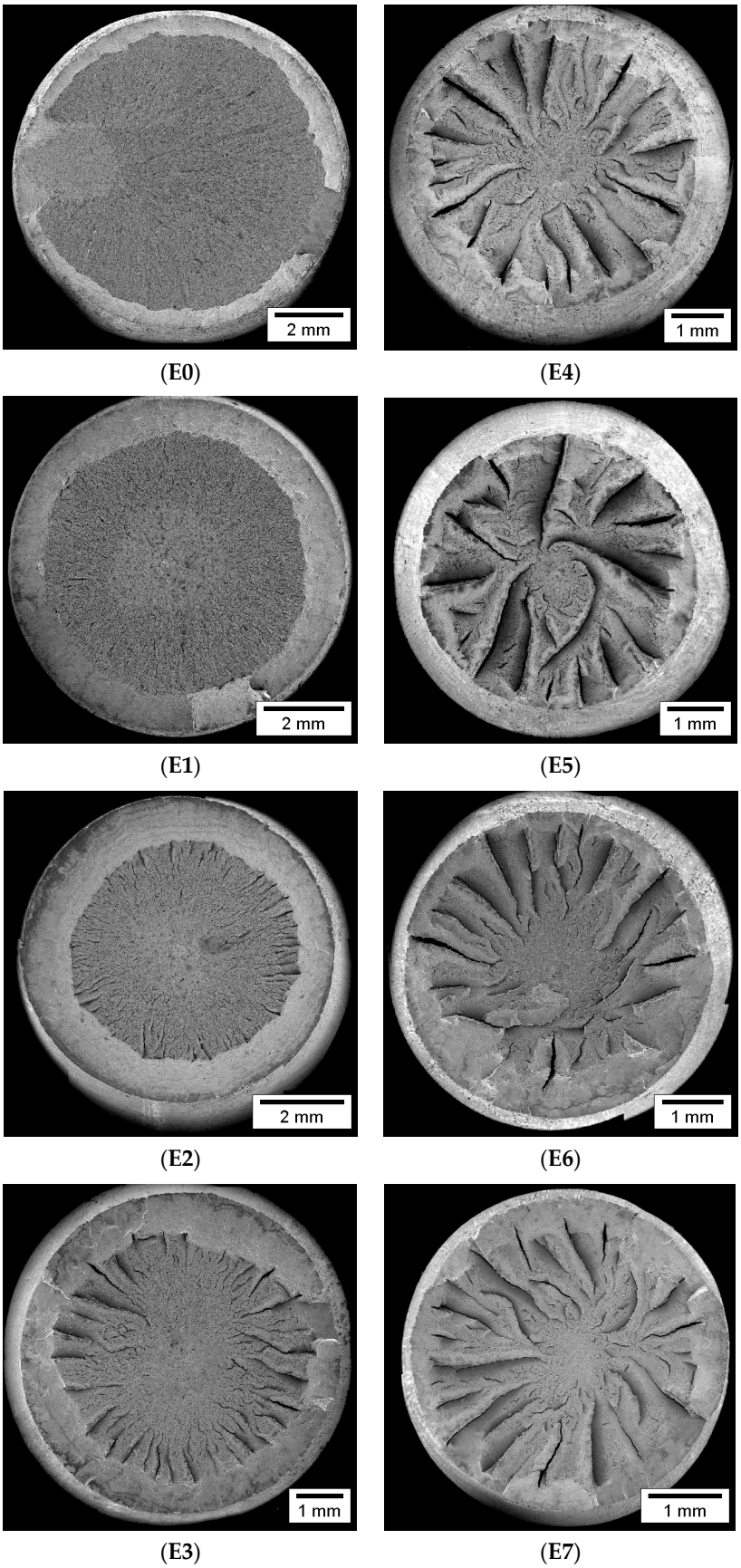

Figure 10. Evolution with drawing of MFMs of drawn wires corresponding to the family E.

In all steels, fracture initiates in a central fibrous region formed by micro-void coalescence (MVC), this domain representing the fracture process zone (FPZ). In addition to the central zone of the wire with a fibrous aspect, ductile fracture appears in the form of MVC at the periphery of all the wires tested as an external ring (shear lip). The micro-void size at the central zone is higher than that observed in the external ring. In moderately-drawn wires, an intermediate zone between the external ring and the central zone was identified with a mixed fractography of MVC and cleavage (C). Radial marks in the direction from the central zone to the external ring are observed. Therefore, fracture was initiated at the wire centre (central fibrous zone by MVC) and later it propagated in radial direction towards the wire periphery. As the drawing degree increases, the area covered by brittle fracture (cleavage zone) decreases, appearing MVC instead of C. Thus, in heavily drawn wires the observed MFM is constituted in the majority of cases only by MVC.

Attention should be paid to certain exceptions to the previously depicted common trend. For instance, the fibrous zone in the specimen E0 (Figure 10) is placed close to the external ring (peripheral fracture origin). Probably this behavior is caused by surface damage generated in the hot-rolled steel during storage.

MFMs were assembled from the SEM micrographs. Later, a quantitative fractographic analysis of the fracture surfaces was carried out by a commercial image analysis software, paying special attention to the following fracture features (Figure 11):

- Total fracture surface (S_F).
- Surface of the FPZ (S_{FPZ}).
- Radius of the FPZ (r_{FPZ}).
- Surface of the external crown formed by MVC (S_{EC}).
- Mean or average depth (x_m), maximum depth (x_{max}) and minimum depth (x_{min}) of the external crown formed by MVC.

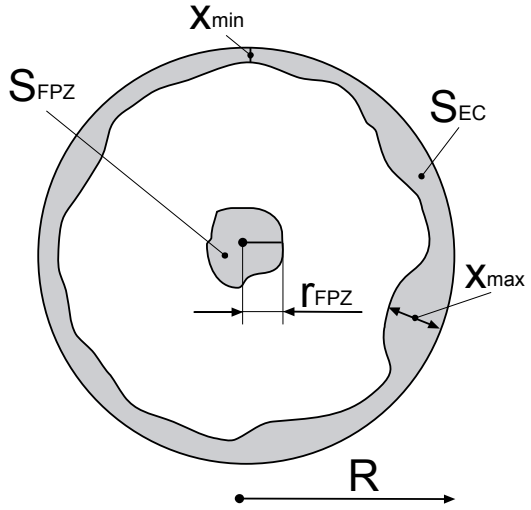

Figure 11. Scheme of the parameters used for defining the fracture surfaces in the quantitative fractographic analysis.

An indicator of the steel ductility (maximum plastic strain undergone by the material up to fracture) is the reduction of the cross sectional area Z. This parameter can be obtained from the initial area of the specimens (S_0) and the final area after fracture (S_F) as follows:

$$Z(\%) = \left(\frac{S_0 - S_F}{S_0} \right) \times 100 \quad (2)$$

The value of the areas of the FPZ (S_{FPZ}) and the external crown (S_{EC}) were measured in terms of the whole fracture area S_F. Accordingly, the radius of the FPZ (r_{FPZ}) and the average depth of the external ring (x_m) were obtained in terms of the radius R of the fractured area by means of the following equations:

$$S_{FPZ}(\%) = \left(\frac{S_{FPZ}}{S_F}\right) \times 100 \quad (3)$$

$$S_{EC}(\%) = \left(\frac{S_{EC}}{S_F}\right) \times 100 \quad (4)$$

$$r_{FPZ}(\%) = \left(\frac{r_{FPZ}}{R}\right) \times 100 \quad (5)$$

$$x_m(\%) = \left(\frac{x_m}{R}\right) \times 100 \quad (6)$$

6. Discussion

The evolution of the reduction of the cross sectional area Z with cumulative plastic strain caused by wire drawing for the five drawn steels is shown in Figure 12. Two trends with the drawing degree are observed. On one hand, Z increases with the drawing degree for slightly drawn steels. On the other hand, for heavily-drawn steels the trend is the opposite, *i.e.*, Z decreases with the drawing degree. Surprisingly, for the steel type A, Z still rises with cold drawing even in the last step, just where such a variable decreases in the other steels. This behavior can be explained on the basis of cumulative plastic strain ε^P and the microstructural orientation inside the steels.

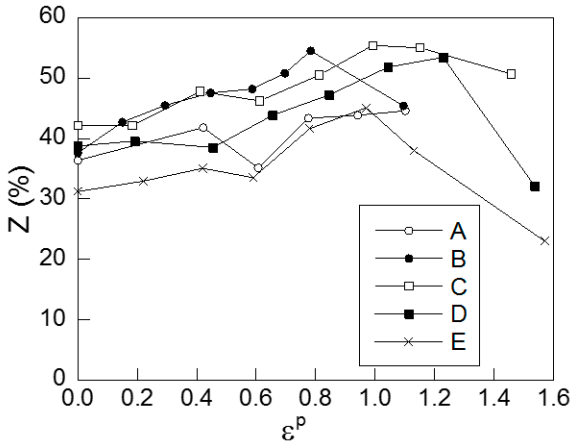

Figure 12. Evolution of the reduction of the cross sectional area with cold drawing.

Mainly, two key consequences appear at the microstructural level in steels as they are drawn: (i) the accumulation of plastic strains and increment of material strength (cold work), and (ii) a microstructure orientation in the wire axial direction. In hot rolled bar (not cold drawn at all), pearlitic colonies (micro-composed of alternated ferrite and cementite lamellae) are randomly oriented. However, as the drawing degree increases, the pearlitic colonies are progressively oriented in the cold drawing direction [13] and the ferrite/cementite lamellae do the same [15], both microstructural levels becoming quasi-aligned with the wire axis or cold drawing direction in the commercial pre-stressing steel wires (final stages of manufacture). The cumulative plastic strain at the end of the drawing chain, *i.e.*, that necessary for the full reorientation in axial direction of both microstructural levels (hierarchical structures of pearlitic colonies and ferrite/cementite lamellae) ranges between 1.1 and 1.6 for the whole set of steel families analyzed in the present paper. This interval fully agrees with the value of 1.5, reported in the scientific literature [30,31], of the cumulative plastic strain necessary for the aforementioned completion of reorientation.

Once the microstructure (colonies and lamellae) are completely oriented in the drawing direction [13,15], the percentage of reduction of the cross sectional area Z begins to decrease, independently of the plastic strain increment (e.g., step 6 to 7 in family types B, C, D and E). The Z reduction is linked with the strong decrease of the interlamellar spacing caused during the microstructure re-orientation at the final stages of drawing [14] and the dislocation density rises in the ferrite lamellae, thus increasing the microstructural packing closeness and reducing the free path for dislocation movement during strain hardening of the progressively drawn steels.

The FPZ (fibrous zone) was characterized by means of its size S_{FPZ} represented in Figure 13, and by its characteristic length r_{FPZ} shown in Figure 14. As a common trend, in all analyzed steel families the two parameters decrease with cold drawing. Figure 15 shows the evolution with the drawing degree of the area of the external crown S_{EC}. It increases up to the second step of the cold drawing process and then continuously decreases as ε^P rises (with certain exceptions in the last step). With regard to its average depth (Figure 16), similar results were obtained for the different steel families.

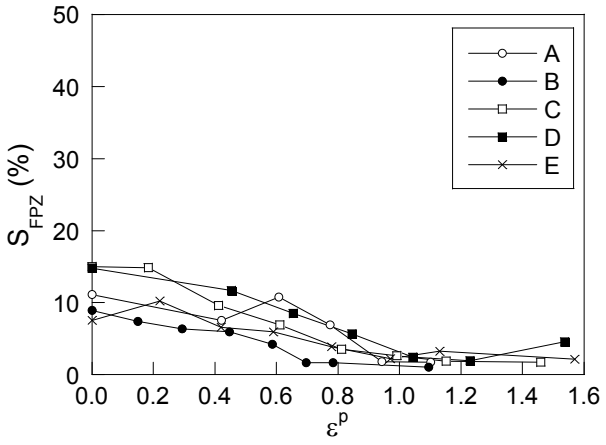

Figure 13. Evolution of the area of the FPZ with the drawing degree.

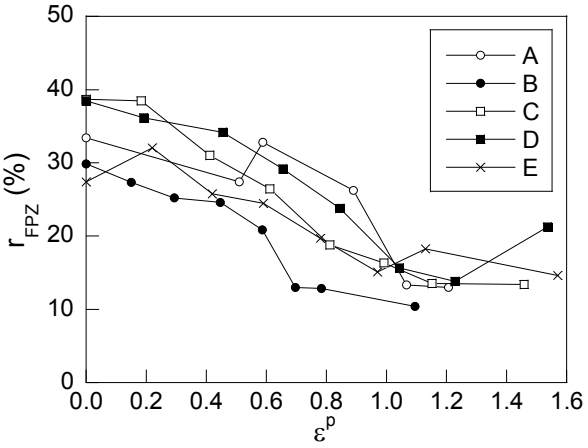

Figure 14. Evolution of radius of the FPZ with the drawing degree.

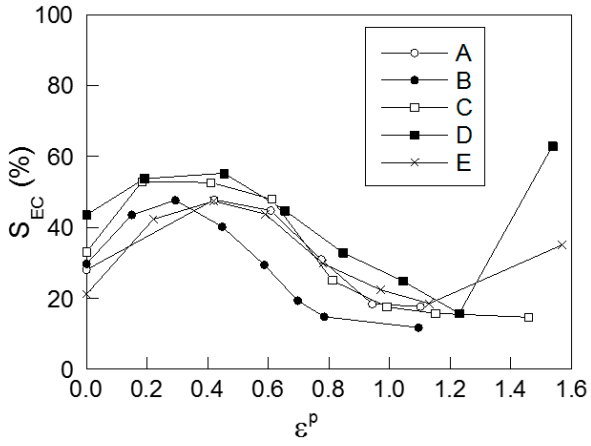

Figure 15. Evolution of the area of the external crown with the drawing degree.

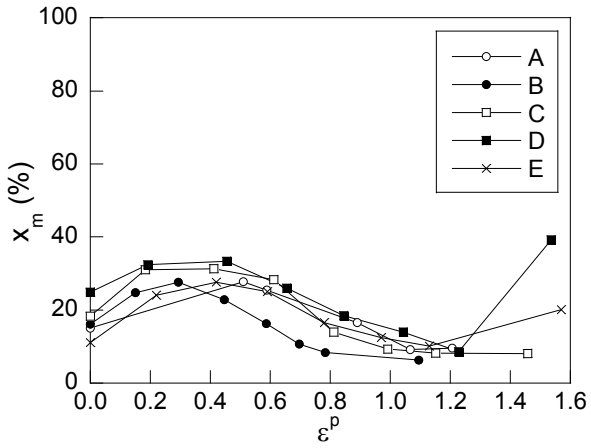

Figure 16. Evolution of the average depth of the external crown with the drawing degree.

7. Conclusions

The fracture surfaces of samples corresponding to very diverse steels, with different cumulative plastic strain, were studied by means of scanning electronic microscope (SEM) and image analysis techniques. In all steels a similar fracture behavior was observed:

- The fracture initiates at the central zone of each wire in which the fracture microscopic topography may be classified as micro-void coalescence (MVC) with fibrous aspect and propagates in a radial direction through the intermediate zone up to reaching the external ring.
- The intermediate zone shows a fractography by cleavage and MVC. The fracture surface by cleavage diminishes in favor of MVC in the last steps of the manufacturing process by cold drawing, so that the fracture process becomes more ductile as the drawing degree increases.
- Another important characteristic of such an intermediate zone is the presence of radial cracks oriented quasi-parallel to the drawing axis or cold drawing direction, embryos of anisotropic fracture behavior as a consequence of manufacture-induced microstructural orientation.
- With regard to the percentage values of the different parts in the fracture surface, the evolution with cold drawing of the central zone of the fibrous aspect (fracture process zone or FPZ) is similar in all analyzed steels and the same happens in the matter of the external ring (shear lip).

Acknowledgments: The authors wish to acknowledge the financial support provided by the following Spanish Institutions: Ministry for Science and Technology (MICYT; Grant MAT2002-01831), Ministry for Education and

Science (MEC; Grant BIA2005-08965), Ministry for Science and Innovation (MICINN; Grant BIA2008-06810), Ministry for Economy and Competitiveness (MINECO; Grant BIA2011-27870), Junta de Castilla y León (JCyL; Grants SA067A05, SA111A07 and SA039A08), and the steel supplied by EMESA TREFILERÍA (*La Coruña, Galicia, Spain*) and TREFILERÍAS QUIJANO (*Los Corrales de Buelna, Santander, Spain*).

Author Contributions: J.T. conceived and designed the experimental procedure; F.J.A., B.G., J.C.M., D.V. and M.L. performed the tests; all the authors analyzed the results and wrote the paper.

Conflicts of Interest: The authors declare no conflict of interest.

Abbreviations

The following abbreviations are used in this manuscript:

FPZ	Fracture Process Zone
SEM	Scanning Electron Microscopy
MFM	Micro-Fracture Map
MVC	Micro-Void Coalescence

References

1. Tao, Z. Mechanical properties of prestressing steel after fire exposure. *Mater. Struct.* **2015**, *48*, 3037–3047. [CrossRef]
2. Hredil, M.I.; Toribio, J. Corrosion resistance of prestressing steel wires. *Mater. Sci.* **2015**, *50*, 665–670. [CrossRef]
3. Jin, X.; Wen, Z.; Xiao, X.; Zhou, Z. A numerical method for prediction of curved rail wear. *Multibody Syst. Dyn.* **2007**, *18*, 531–557. [CrossRef]
4. Ostash, O.P.; Andreiko, I.M.; Kulyk, V.V.; Vavrukh, V.I. Influence of braking on the microstructure and mechanical behavior of railroad wheel steels. *Mater. Sci.* **2013**, *48*, 569–574. [CrossRef]
5. Christodoulou, I.A.; Kermanidis, A.T.; Haidemenopoulos, G.N. Fatigue and fracture behavior of pearlitic Grade 900A steel used in railway applications. *Theor. Appl. Fract. Mech.* **2016**, *83*, 51–59. [CrossRef]
6. Gamboa, E.; Atrens, A. Material influence on the stress corrosion cracking of rock bolts. *Eng. Fail. Anal.* **2005**, *12*, 201–235. [CrossRef]
7. Lee, S.K.; Ko, D.C.; Kim, B.M. Pass schedule of wire drawing process to prevent delamination for high strength steel cord wire. *Mater. Des.* **2009**, *30*, 2919–2927. [CrossRef]
8. Bramfitt, B.L.; Mridha, S. Steels: Near Eutectoid. In *Reference Module in Materials Science and Materials*; Hashmi, M.S.J., Ed.; Elsevier: Amsterdam, The Netherlands, 2016.
9. Toribio, J.; Lorenzo, M.; Vergara, D.; Kharin, V. Hydrogen degradation of cold-drawn wires: A numerical analysis of drawing-induced residual stresses and strains. *Corrosion* **2011**. [CrossRef]
10. Elices, M. Influence of residual stresses in the performance of cold-drawn pearlitic wires. *J. Mater. Sci.* **2004**, *39*, 3889–3899. [CrossRef]
11. Toribio, J.; Kharin, V.; Lorenzo, M.; Vergara, D. Role of drawing-induced residual stresses and strains in the hydrogen embrittlement susceptibility of prestressing steels. *Corros. Sci.* **2011**, *53*, 3346–3355. [CrossRef]
12. Toribio, J.; Ovejero, E. Microstructure evolution in a pearlitic steel subjected to progressive plastic deformation. *Mater. Sci. Eng. A* **1997**, *234–236*, 579–582. [CrossRef]
13. Toribio, J.; Ovejero, E. Microstructure orientation in a pearlitic steel subjected to progressive plastic deformation. *J. Mater. Sci. Lett.* **1998**, *17*, 1037–1040. [CrossRef]
14. Toribio, J.; Ovejero, E. Effect of cumulative cold drawing on the pearlite interlamellar spacing in eutectoid steel. *Scr. Mater.* **1998**, *39*, 323–328. [CrossRef]
15. Toribio, J.; Ovejero, E. Effect of cold drawing on microstructure and corrosion performance of high-strength steel. *Mech. Time-Depend. Mater.* **1998**, *1*, 307–319. [CrossRef]
16. Zelin, M. Microstructure evolution in pearlitic steels during wire drawing. *Acta Mater.* **2002**, *50*, 4431–4447. [CrossRef]
17. Sauvage, X.; Guelton, N.; Blavette, D. Microstructure evolutions during drawing of a pearlitic steel containing 0.7 at. % copper. *Scr. Mater.* **2002**, *46*, 459–464. [CrossRef]
18. Guo, N.; Luan, B.; Wang, B.; Liu, Q. Deformation bands in fully pearlitic steel during wire drawing. *Sci. China Technol. Sci.* **2014**, *57*, 796–803. [CrossRef]

19. Fang, F.; Zhao, Y.; Liu, P.; Zhou, L.; Hu, X.J.; Zhou, X.; Xie, Z.H. Deformation of cementite in cold drawn pearlitic steel wire. *Mater. Sci. Eng. A* **2014**, *608*, 11–15. [CrossRef]
20. Zhang, X.; Godfrey, A.; Huang, X.; Hansen, N.; Liu, Q. Microstructure and strengthening mechanisms in cold-drawn pearlitic steel wire. *Acta Mater.* **2011**, *59*, 3422–3430. [CrossRef]
21. Fang, F.; Zhou, L.; Hu, X.; Zhou, X.; Tu, Y.; Xie, Z.; Jiang, J. Microstructure and mechanical properties of cold-drawn pearlitic wires affect by inherited texture. *Mater. Des.* **2015**, *79*, 60–67. [CrossRef]
22. Rastegari, H.; Kermanpur, A.; Najafizadeh, A. Effect of initial microstructure on the work hardening behavior of plain eutectoid steel. *Mater. Sci. Eng. A* **2015**, *632*, 103–109. [CrossRef]
23. Toribio, J.; Kharin, V.; Ayaso, F.J.; González, B.; Matos, J.C.; Vergara, D.; Lorenzo, M. Numerical and experimental analyses of the plasticity-induced fatigue crack growth in high-strength steels. *Const. Build. Mater.* **2011**, *25*, 3935–3940. [CrossRef]
24. Toribio, J.; Matos, J.C.; González, B. A macro- and micro-approach to the anisotropic fatigue behaviour of hot-rolled and cold-drawn pearlitic steel. *Eng. Fract. Mech.* **2014**, *123*, 70–76. [CrossRef]
25. Toribio, J.; Ayaso, F.J.; González, B.; Matos, J.C.; Vergara, D.; Lorenzo, M. Critical stress intensity factors in steel cracked wires. *Mater. Des.* **2011**, *32*, 4424–4429. [CrossRef]
26. Toribio, J.; González, B.; Matos, J.C. Strength anisotropy and mixed mode fracture in heavily drawn pearlitic steel. *Fat. Fract. Eng. Mater. Struct.* **2013**, *36*, 1178–1186. [CrossRef]
27. Toribio, J.; Vergara, D.; Lorenzo, M. Influence of loading rate on the hydrogen-assisted micro-damage in bluntly notched samples of pearlitic steel. *Metals* **2016**, *6*, 11. [CrossRef]
28. Meseguer-Valdenebro, J.L.; Miguel, V.; Caravaca, M.; Portolés, A.; Gimeno, F. Teaching mechanical properties of different steels for engineering students. *J. Mater. Educ.* **2015**, *37*, 103–118.
29. Toribio, J. On the intrinsic character of the stress-strain curve of a prestressing steel. *J. Test. Eval.* **1992**, *20*, 357–362. [CrossRef]
30. Zhang, X.; Godfrey, A.; Hansen, N.; Huang, X.; Liu, W.; Liu, Q. Evolution of cementite morphology in pearlitic steel wire during wet wire drawing. *Mater. Charact.* **2010**, *61*, 65–72. [CrossRef]
31. Zhang, X.; Godfrey, A.; Hansen, N.; Huang, X. Hierarchical structures in cold-drawn pearlitic steel wire. *Acta Mater.* **2013**, *61*, 4898–4909. [CrossRef]